2003 ANNUAL REPORT

FUSION RESEARCH CENTER

GEORGIA INSTITUTE OF TECHNOLOGY

(INCLUDING ANNUAL REPORTS FOR DOE GRANTS

DE-FG0296ER54350 & DE-FG02-ER54538)

W. M. STACEY

J. MANDREKAS

DECEMBER, 2003

I. NEXT-STEP OPTION DESIGN STUDIES (DOE GRANT ER54350)

A. *FUSION TRANSMUTATION OF NUCLEAR WASTE*

We are investigating the potential applications of fusion neutron sources to 'drive' sub-critical fission reactors to perform one or more possible 'nuclear' missions. Our work indicates that since only a fraction of the neutrons in these applications would be fusion neutrons, the requirements are modest relative to the requirements for pure fusion electrical power (e.g. for the transmutation mission-- fusion power $P_{fus} \leq 250$ MW, fusion power density $\beta_N \leq 2.5$, 14 MeV neutron wall load $\Gamma_n < 1$ MW/m^2 and power amplification $Q_p \leq 2$). We believe on the basis of our studies that by making use of ITER physics and technology, using ITER as a prototype, and adopting the reactor and processing technology being developed in the nuclear program could lead to a fusion-driven sub-critical reactor for the transmutation of spent nuclear fuel, fissile breeding or disposition of weapons-grade plutonium being on-line by 2040, as compared to the plans for putting critical and accelerator-driven sub-critical reactors on-line for such missions by 2030. All of the R&D needed to develop the fusion neutron source for such a facility is directly on the path to fusion power (in fact is needed for an electric power DEMO); and the operation of a fusion-driven sub-critical reactor could also serve the purposes envisioned for a 'volume neutron source', thus taking the place of such a device in the development path to fusion power.

Tokamak Neutron Source Requirements

We have performed a series of systems studies[1-4] to examine whether a tokamak neutron source for a sub-critical transmutation reactor could be designed using the existing physics and fusion technology databases. Such a tokamak neutron source would be based on the ITER physics design basis and on the ITER first-wall, divertor, heating-current drive, tritium, etc. systems, but would likely use a liquid metal coolant for compatibility with the transmutation reactor and a ferritic steel structural material of the type being developed for nuclear applications. Two variants were examined—the FTWR (fusion transmutation of waste reactor) with copper magnet systems and the FTWR-SC with essentially the ITER superconducting magnet systems. A third variant based on advanced tokamak (AT) physics and the ITER superconducting magnet system—the FTWR-AT—was also examined. The principal parameters of such tokamak neutron sources are given in Table 1. The fusion powers shown in Table 1 correspond to the indicated value of β_N and the plasma volume; smaller values would result from operating at lower β_N.

Table 1 Tokamak Neutron Source Parameters for Transmutation Reactors

Parameter	FTWR[a]	FTWR-SC[b]	FTWR-AT[c]	ITER[d]
Fusion power, P_{fus} (MW)	≤ 150	≤ 225	≤ 500	410
Neutron source, $S_{fus}(10^{19}$ #/s)	≤ 5.3	≤ 8.0	≤ 17.6	14.4
Major radius, R (m)	3.1	4.5	3.9	6.2
Minor radius, a (m)	0.9	0.9	1.1	2.0
Elongation, κ	1.7	1.8	1.7	1.8
Current, I (MA)	7.0	6.0	8.0	15.0
Magnetic field, B (T)	6.1	7.5	5.7	5.3
Confinement, H(y,2)	1.1	1.0	1.5	1.0
Normalized beta, β_N	≤ 2.5	≤ 2.5	4.0	1.8
Plasma Power Mult., Q_p	≤ 2.0	≤ 2.0	4.0	10
Electric Power Mult, Q_e	1	5		
Current-drive effic. η_{cd}	0.03	0.024	0.05	
" , $\gamma_{cd}(10^{-20}$ A/Wm^2)	0.19	0.20	0.28	
Bootstrap I fraction, f_{bs}	0.67(0.38)[e]	0.56(0.24)	0.25	
Neut. flux, Γ_n (MW/m^2)	≤ 0.8	≤ 1.0	≤ 1.7	0.5
Heat flux, q_{fw} MW/m^2)	≤ 0.4	≤ 0.3	≤ 0.5	0.15
Availability (%)	≥ 50	≥ 50	≥ 50	

[a] ITER physics, liquid nitrogen cooled copper magnets.(Ref. 2)
[b] ITER physics, superconducting magnets. (Ref. 3)
[c] AT physics, superconducting magnets. (Ref. 4)
[d] ITER design parameters. (Ref. 5)
[e] required (estimated from present database)

For the FTWR and FTWR-SC, the requirements on β_N and confinement are within the present experimental range, and the requirements on β_N, confinement, energy amplification Q_p, and fusion power level are at or below the ITER level. The requirement on the combination of current-drive efficiency and bootstrap current fraction is beyond what has been achieved to date, but is certainly within the range envisioned for AT operation and may be achieved in ITER. Actually, the advanced current drive capability is the only AT operating capability that is needed or that can be taken advantage of for a fusion neutron source for the transmutation mission.

The configuration of the three FTWR concepts is depicted in Fig. 1. The sub-critical reactor is in the form of an annulus 40 cm thick by 228 cm high that wraps about the outboard side of the plasma chamber. This reactor is composed of fast reactor fuel assemblies containing 0.6 cm pins of a zirconium alloy containing transuranics from the SNF dispersed in a zirconium matrix. The reactor coolant is a lithium-lead eutectic enriched in ^{6}Li to achieve tritium self-sufficiency. A reflector and shield are located inboard of, above, and below the plasma chamber and above, below and outboard of the reactor to protect the magnets from radiation damage and to reflect neutrons towards the reactor. The magnet systems for the FTWR used oxygen-free high conductivity copper conductor and liquid nitrogen coolant, and the magnet systems for the FTWR-SC and FTWR-AT used Nb_3Sn and NbTi conductor cooled by supercritical helium.

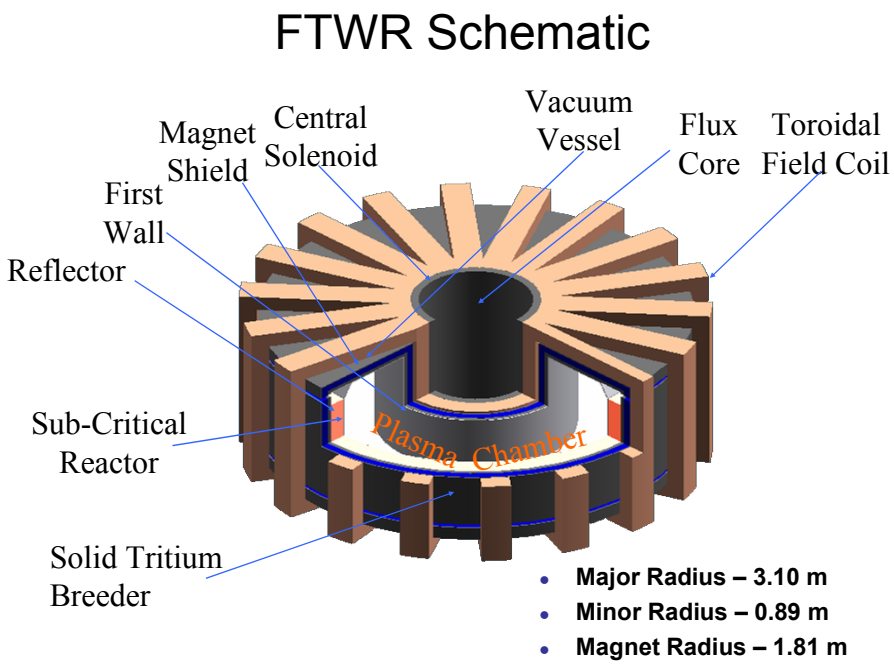

Figure 1 : Tokamak Fusion Transmutation of Waste Reactor

Nuclear Analysis

The nuclear transmutation reactor used for these studies was a metal fueled, Pb-Li cooled fast reactor adapted from an Argonne National Laboratory design of a transmutation reactor. We carried out a series of calculations to confirm the nuclear performance and to evaluate the safety characteristics of this reactor in the configuration of Fig. 1. These results[6] indicated that a subcritical reactor may be able to operate with a purely transuranic fuel, which would result in a higher net transmutation rate than a critical reactor operating at the same power level (because of the necessity of including U-238 to provide negative reactivity feedback in a critical reactor but also to cause the production of additional transuranics).

Comparative nuclear transmutation fuel cycle analyses of the FTWR, of a similar accelerator-driven sub-critical reactor, and of a similar critical reactor (but with U-238 included in the fuel) were performed[7]. The two subcritical reactors were found to have better overall transmutation performance than the critical reactor.

Incorporation of Transmutation Mission into the Fusion Development Program

The transmutation mission can be carried out with a tokamak fusion neutron source based on physics (H, β_N, Q_p, etc.) similar to or less demanding than that used for the ITER design, so the R&D program supporting ITER and the electrical power development mission will suffice for a transmutation neutron source in most physics areas. However, the transmutation neutron source would need to achieve a higher bootstrap current fraction and/or higher current drive efficiency and to achieve quasi-steady state operation in order to achieve higher availability than ITER. These issues must be addressed prior to the DEMO in the electrical power development path, but would have a higher relative priority in a physics R&D program for the transmutation mission.

The transmutation fusion neutron source can be constructed with the fusion technology being developed for ITER, for the most part, so the technology R&D supporting ITER will also support the fusion neutron source. However, the fusion neutron source will need to achieve greater availability, hence have greater component reliability, than ITER. The issue of component reliability, which will require various component test facilities, must be addressed prior to the DEMO in the electric power development path, but would have a higher relative priority in a technology development program to support the transmutation mission.

The reactor technology for the sub-critical reactor driven by the fusion neutron source should logically be adapted from the reactor (nuclear, fuel, cooling, processing, materials) technologies being investigated in the nuclear program (e.g. those being considered in the Generation–IV[8] and other such studies), but these technologies must be modified to provide for the tritium breeding requirement. A fusion nuclear technology program would have to be revived with this goal. There is a need to develop a long-lived structural material, primarily for the fuel assemblies of the sub-critical reactor but also for the first wall of the fusion neutron source, but it may be possible to build the initial transmutation fusion neutron sources with austenitic stainless steel first walls.

The technical requirements for a tokamak fusion neutron source that would fulfill the transmutation mission are significantly less demanding than for an economically competitive tokamak electrical power reactor, as indicated in Table 2. The first such neutron source could be built immediately following ITER, either before or in parallel with a fusion electrical power demonstration reactor (DEMO), which would have more demanding technical requirements on β_N, confinement and Q_p.

A more comprehensive systems/conceptual design investigation of the application of fusion to the transmutation mission is planned to further evaluate the possibility of incorporating a transmutation mission into the fusion development program. Evaluation of the competitiveness of sub-critical reactors driven by fusion neutron sources for the transmutation of SNF and of the required R&D would be the objectives of these studies. These investigations will initially be based on the most developed tokamak confinement concept (using the ITER physics and technology databases) and on adaptation of the reactor technology being developed in the nuclear program. Such studies will be coordinated with the GEN-IV nuclear fuel cycle studies[8].

We intend to next investigate a gas-cooled fast transmutation reactor using the TRISO fuel pellet that will be further developed in the nuclear program[11]. This type of fuel provides the potential for achieving almost complete transmutation of the actinides in spent nuclear with a minimal number of separation and reprocessing steps.

Table 2 Requirements for a Tokamak Neutron Source for a Transmutation Reactor, for an Economically Competitive Fusion Electric Power Tokamak Reactor and for a Tokamak DEMO

Parameter	Transmutation	Electric Power[a]	DEMO[b]
Confinement H(y,2)	1.0	1.5-2.0	1.5-2.0
Beta β_N	< 2.5	> 5.0	> 4.0
Power Amplification Q_p	< 2	≥ 50	> 10
Bootstrap Current Fraction f_{bs}	0.2-0.4	0.9	0.7
Neutron wall load (MW/m^2)	< 1.0	> 4.0	> 2.0
Fusion Power (MW)	≤ 200	3000	1000
Pulse length/duty factor	long/steady-state	long/steady-state	long/steady-state
Availability (%)	≥ 50	90	≥ 50

[a] ARIES studies (Ref. 9); [b] DEMO studies (Ref. 10)

1. W. M. Stacey, "Capabilities of a DT Tokamak Fusion Neutron Source for Driving a Spent Nuclear Fuel Transmutation Reactor", *Nucl. Fusion,* **41**, 135 (2001).
2. W. M. Stacey, J. Mandrekas, E. A. Hoffman, et al., "A Fusion Transmutation of Waste Reactor", *Fusion Sci. Technol.,* **41**, 116 (2002).
3. A. N. Mauer, W. M. Stacey, J. Mandrekas and E. A. Hoffman, "A Superconducting Fusion Transmutation of Waste Reactor", *Fusion Sci. Technol.,* to be published (2004).
4. J. Mandrekas, L. A. Cottrill, G. C. Hahn and W. M. Stacey, "An Advanced Tokamak Neutron Source for a Fusion Transmutation of Waste Reactor", Georgia Tech report GTFR-167 (2003).
5. ITER website www.iter.org .
6. E. A. Hoffman and W. M. Stacey, "Comparative Fuel Cycle Analysis of Critical and Subcritical Fast Reactor Transmutation Systems", *Nuclear Technol.*, **144**, 83 (2003).
7. E. A. Hoffman and W. M. Stacey, "Nuclear Design and Analysis of the Fusion Transmutation of Waste Reactor", *Fusion Sci. Technol.*, to be published (2004).
8. GEN-IV roadmap website http://gif.inel.gov/roadmap/.
9. ARIES web site aries/ucsd.edu/aries.
10. W. M. Stacey, "Tokamak Demonstration Reactors", *Nucl. Fusion*, **35**, 1369 (1995).
11. D. A. Petti, et al., "Key Differences in the Fabrication, Irradiation and High Temperature Accident Testing of US and German TRISO-Coated Particle Fuel, and Their Implications on Fuel Performance", *Nucl. Eng. Des*., 222, 281 (2003).

B. FUSION IGNITION RESEARCH EXPERIMENT

(J. Mandrekas)

During FY2003, the Georgia Tech Fusion Research Center continued its participation in the physics design activities of the Fusion Ignition Research Experiment (FIRE). Our main focus has been transport simulations with our 1½-D main plasma – multi charge state impurity transport code GTWHIST[1], in order to evaluate the impact of impurity seeded operation on the performance of FIRE.

While the new FIRE divertor design[2] can withstand the anticipated heat loads from the plasma core during the standard ELMy H-mode operation of the device, enhanced radiation from seeded impurities from the plasma mantle and the divertor is expected to be necessary during the higher power Advanced Tokamak (AT) operating mode in order to maintain a flexible operating space.

As a first step, the entire* FIRE reference operating scenario was modeled with GTWHIST and compared to the reference TSC simulation[3]. The results of this benchmarking simulation are shown in Fig,2, where time histories of various global power quantities are plotted. A fixed-shape transport model normalized to yield an H-factor of about 1 relative to the ITER IPB(y,2) global confinement scaling was adopted for these simulations.

* Since the MHD part of the GTWHIST code supports fixed-boundary configurations only, our simulation starts when the plasma geometry and fields (major and minor radii and toroidal magnetic field) are at their reference values, corresponding to about 4 seconds in the TSC simulation.

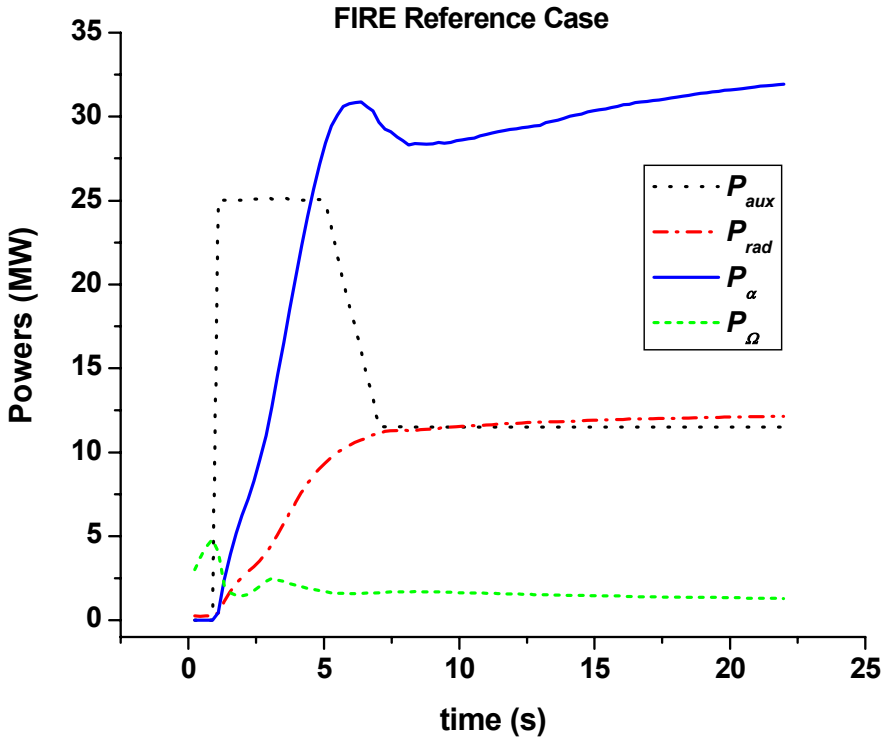

Figure 2: GTWHIST evaluation of the time history of various global power balance parameters for the FIRE reference case.

Following the establishment of the reference discharge, Argon impurities were injected at the edge of the device and their evolution and contribution to the power balance were followed using the multi-charge state impurity transport capabilities of the GTWHIST code. A fixed diffusion coefficient of 0.5 m^2/s for all impurity charge states and no inward pinch have been assumed in these simulations. The profiles of the various Ar charge states are shown in Fig. 3, for a 0.3% global Ar concentration.

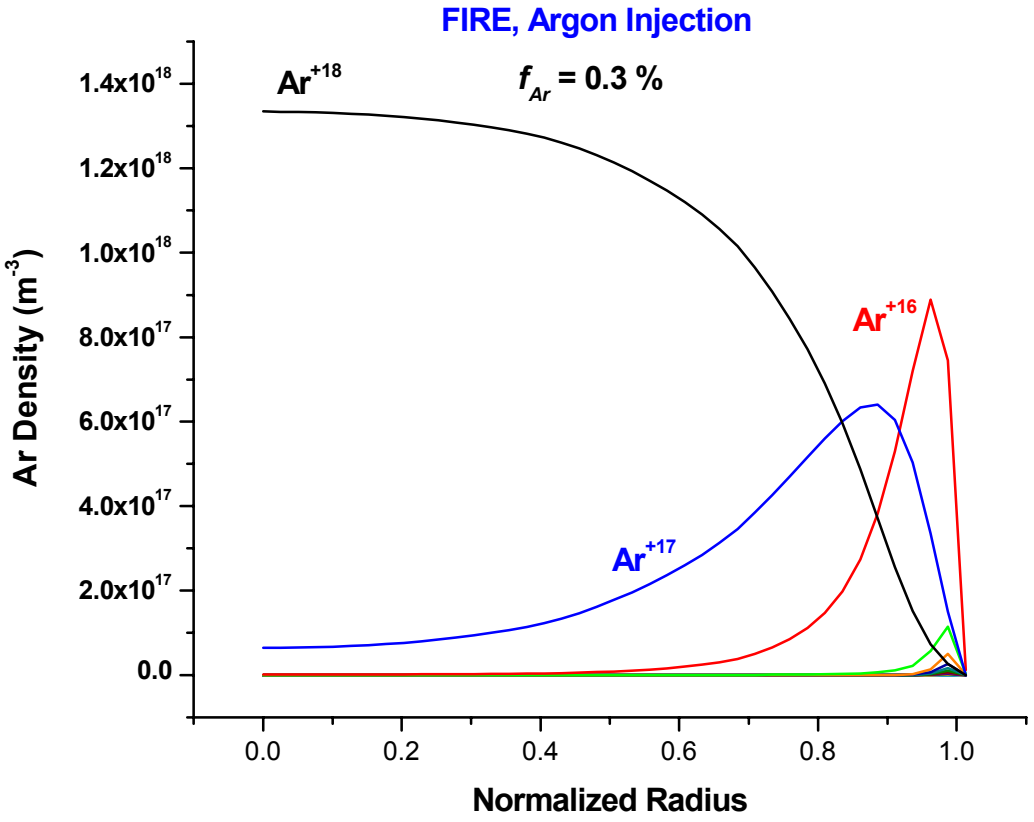

Figure 3: Profiles of Argon charge states following Ar injection.

As expected, Ar is almost fully ionized in the plasma core, while the highly radiating Lithium-like and Helium-like charge states are concentrated in the plasma edge. Our simulation predicts that for the reference concentration of 0.3%, the total radiated power by the Ar impurities (including bremsstrahlung and line radiation) is 45.2 MW, which is about 20%-30% higher than the predictions of earlier 0-D (fixed profiles) simulations. This suggests that lower Ar concentrations may be adequate to meet the needs of the FIRE design.

In addition to the determination of the radiating properties of the seeded Ar impurities, our simulations identified a number of critical issues that must be addressed before impurity seeding can be safely adopted as part of the reference operating scenario of FIRE. These include: a) the potential of edge thermal instabilities following Ar injection which were observed in several of our simulations and which can collapse the edge temperature profile and, eventually, terminate the plasma; b) the sensitivity of our predictions to the edge temperature assumptions, underlying the need for a realistic and accurate pedestal boundary condition model; c) the importance of the edge ion and electron thermal transport assumptions; and d) the possibility of core impurity accumulation due to neoclassical effects arising from peaked density profiles. These issues will be examined in detail during our FY2004 FIRE work.

1. J. Mandrekas, W. M. Stacey, F. A. Kelly, "Impurity Seeded Radiative Power Exhaust Solutions for ITER", *Nucl. Fusion*, **36**, 917 (1996).

2. M. Ulrickson, et al., "Issues and Recent Advances on PFCs for ITER and FIRE", Bull. Am. Phys. Soc., **48** 343 (2003).
3. C. Kessel, PPPL, personal communication, Dec. 2003.

C. SUPPORT FOR NTCC ACTIVITY

(J. Mandrekas)

During FY 2003, we continued our participation in the National Transport Code Collaboration (NTCC) activity. We completed the review of the neutral transport module NUT (P. Valanju, IFS) and are in the process of upgrading the Lower Hybrid module LSC (D.W. Ignat, PPPL) with the addition of trapped electron effects. The upgraded module will be benchmarked against lower hybrid current drive simulations by P. Bonoli of MIT, and will then be resubmitted to the NTCC for eventual review and acceptance in the module library.

II. ANALYSIS OF DIII-D EXPERIMENTS (DOE GRANT ER54538)

A. TRANSPORT IN THE EDGE PEDESTAL

(W. M. Stacey and R. J. Groebner)

Theoretical heat conductivities based on analytical representations of neoclassical and ITG modes for the ions and ETG and TEM modes for the electrons have been compared with measured transport rates in the edge pedestal for several DIII-D shots with a wide range of edge parameters. Thermal transport coefficients from the neoclassical, ITG and ETG theories are found to be within at most a factor of 2-3 of values inferred from experiment for most of the discharges considered, as shown in Table 1.

Table 1: Experimental and theoretical thermal conductivities (m^2/s)

Shot	ν_e^*	L_{Ti}/L_{Ti}^{crit}	η_e	$\chi_i^{exp,a}$	χ_i^{NEO}	χ_i^{ITG}	$\chi_e^{exp,a}$	χ_e^{TEM}	χ_e^{ETG}
93045	0.10	0.27	1.03	0.20	0.31(0.67[b])	3.7	0.17	>100	2.4
87085	0.28	0.49	0.96	1.1	0.58(0.93)	2.5	1.4	52	3.6
97979	0.40	0.36	1.27	0.80	0.49(0.54)	1.7	0.48	44	1.6
106005	0.30	0.31	1.29	1.1	0.62(0.76)	1.7	0.57	62	2.8
106012	0.62	0.60	1.20	1.6	0.51(0.67)	0.59	0.73	21	1.5
92976	1.53	0.60	1.43	1.5	0.53(0.84)	0.37	1.3	1.6	1.4
98893	4.86	0.59	1.00	1.0	0.62(0.68)	0.20	0.34	1.7	0.55

[a] Experimental values evaluated assuming $Q_i = Q_e$.
[b] Without orbit squeezing correction.

The edge gradients of these discharges are such that ITG and ETG modes are predicted to be unstable. This finding that ETG modes should be unstable in the edge is consistent with previous observation of $\eta_e \approx 2$ in a large number of discharges in ASDEX Upgrade[1]. Furthermore, the results shown in Fig. 16 of Ref. 2 imply that $\eta_e \approx 1.5$ in a large number of DIII-D discharges.

New expressions for a 'diffusive-pinch' form of particle flux, for calculating an experimental frequency for momentum transfer, and for predicting the density gradient scale length have been derived from momentum balance. The experimental momentum transfer rates are too large by an order of magnitude to be accounted for by atomic physics and convective momentum transfer, but neoclassical gyroviscous theory predicts frequencies comparable to those found experimentally.

The new expression for the density gradient scale length of ion species 'j' is

$$L_{nj}^{-1} = \frac{e_j B_\theta}{n_j m_j \nu_{dj}^* T_j}\left[e_j B_\theta \Gamma_j + M_{\phi j} + n_j e_j E_\phi^A - n_j m_j \nu_{jk}\left(\upsilon_{\phi j} - \upsilon_{\phi k}\right)\right] - \frac{e_j B_\theta}{T_j}\left(f_p^{-1}\upsilon_{\theta j} + \frac{E_r}{B_\theta}\right) - L_{Tj}^{-1} \quad (1)$$

We find that the momentum input (M_φ) and toroidal electric field (E_φ) contributions are negligible and would expect that the friction term can also be neglected. The import of Eq. (1) is then that the pressure gradient scale length is determined by the particle flux (Γ) and momentum transfer rate (ν_d*), by the poloidal rotation, and by the radial electric field, which latter is related to both poloidal and toroidal rotation velocities. Since the temperature gradient scale length is determined by heat transport, the density gradient scale length must adjust to satisfy this momentum balance constraint on the pressure gradient. We expect these transport constraints to govern the pedestal gradient scale lengths between or in the absence of ELMs.

We evaluated an average value of the gradient scale length from Eq. (1) for the main ion species as follows. The momentum transfer frequency was calculated from the neoclassical expression[3] plus the atomic physics and convective momentum transfer frequencies. The radial particle flux was determined from particle balance, and the neutral beam momentum input in the pedestal was calculated directly. The friction term involving the difference in ion and impurity toroidal velocities was assumed to be negligible. The E_φ^A term and the temperature gradient scale length term were evaluated from experimental data. The poloidal velocity was determined by solving coupled Fourier moments of the poloidal momentum balance equation for the poloidal velocities of the ions and impurities and for the sine and cosine components of the ion and impurity density asymmetries which are needed to evaluate the poloidal asymmetry factor needed to evaluate the neoclassical gyroviscous contribution to ν_d*; this calculation is described in detail in Ref. 4. The radial electric field was calculated by summing the toroidal components of the momentum balance equation for the ions and impurities to obtain

$$\frac{E_r}{B_\theta} = \frac{\left\{M_{\phi i} + M_{\phi I}\right\} + n_i m_i \nu_{di}^*\left(P_i' - f_p^{-1}\upsilon_{\theta i}\right) + n_I m_I \nu_{dI}^*\left(P_I' + f_p^{-1}\upsilon_{\theta I}\right)}{n_i m_i \nu_{di}^* + n_I m_I \nu_{dI}^*} \quad (2)$$

and using the theoretical values of ν_{di}*and $\upsilon_{\theta i}$ just discussed, together with the experimental value of P_i'. Density gradient scale lengths calculated from Eq. (1) are within a factor of 2 or closer of those measured directly (Thomson scattering), as shown in Table 2, confirming the consistency of the calculation.

Table 2: Density gradient scale lengths

Shot	93045	87085	97979	106005	106012	92976	98893
Exp. L_n	2.8	4.3	3.3	2.7	2.4	6.0	1.5
Calc. L_n	2.7	3.3	2.4	1.9	1.8	3.3	0.8

Perhaps the most significant finding of this investigation is that neoclassical theory appears to provide a reasonable representation of ion transport in the edge pedestal. The neoclassical predictions of both ion thermal conductivity and ion momentum transfer frequency were within a factor of 2-3 or less of the experimental values, and the use of neoclassical momentum transfer frequencies in the calculation of density gradient scale lengths results in a prediction that is within a factor of 2 of the directly measured value.

A paper has been prepared for Physics of Plasmas, and a presentation was made at APS-DPP-03.

1. J. Neuhauser, D. P. Coster, H. U. Farbach, et al., Plasma Phys. Control. Fusion, 44, 855 (2002).
2. R. D. Deranian, R. J. Groebner and D. T. Pham, Phys. Plasmas, 7, 1235 (2000).
3. W. M. Stacey and D. J. Sigmar, Phys. Fluids, 28, 2800 (1985).
4. W. M. Stacey, Phys. Plasmas, 9, 3874 (2002).

B. L-H POWER THRESHOLD

(W. M. Stacey)

It was shown recently[1] that there is a critical, threshold non-radiative heat flux through the plasma edge above which thermal instabilities with short radial wavelengths[2] are stabilized. This critical heat flux can be represented as a threshold power crossing the separatrix

$$P_{thresh} = \frac{5}{4}\Gamma_\perp T\, A_{sep}\left[\sqrt{1+\frac{\left(\chi^0\left(\alpha-\chi^0 k_r^2\right)/\nu\right)}{\left(\frac{5}{4}\frac{\Gamma_\perp}{n}\right)^2}}+1\right] \qquad (1)$$

where $k_r^{-1} \approx$ 1-10 cm is the radial wavelength of the instability, $\chi_0 \approx 0.1 - 1.0$ m^2/s is the background thermal conductivity in the absence of thermal instabilities, $\nu \approx 3/2 - 7/2$ represents the temperature dependence of $\chi_0 \sim T^\nu$, α represents the temperature dependence of the atomic physics cooling terms, $\Gamma\perp$ is the ion flux crossing the separatrix and A_{sep} is the area of the separatrix.

The predicted phenomena[1]--a decrease in the values of both edge temperature gradient scale length and the heat conductivity associated with the thermal instabilities as the power flux approached the threshold value from below and the sharp decrease in both quantities as the threshold was crossed--were suggestive of the low-to-high (L-H) transition in tokamaks. The predicted phenomena as the power flux approached the threshold value from above were similarly suggestive of the H-L back transition.

A first test of this prediction of a threshold heat flux for the H-L back transition against data from DIII-D was recently made[3] for a set of 'density limit' shots in which the density was increased in H-mode discharges by gas fueling until a H-L mode back transition took place. The increasing density produced increasing core radiation and, at constant heating power, decreasing non-radiative power flowing outward across the separatrix. Good agreement was obtained between the predicted and experimental values of the non-radiative power crossing the separatrix at the time of the H-L back transition for a set of shots with high radiative power fraction. We have now made a similar comparison of predicted and measured values of the non-radiative power crossing the separatrix at the time of the L-H transition for a representative set of DIII-D shots in which the radiative power fraction is small at the time of the transition.

Good agreement has been found between the measured non-radiative power crossing the separatrix just prior to a L-H transition and the sum of the predicted threshold powers for thermal instability stabilization in the ion and electron power balances, for a set of shots with core radiative power fractions of 10% or less, as shown in Table 1. The calculation is relatively insensitive to the exact value of k_r^{-1}, χ_0 , or ν in the above ranges.

Table 1 Some DIII-D shots just prior to the L-H transition (R=1.71-1.79m, a=0.6m, κ=1.73-1.89, LSN divertor)

Shot #	Time (ms)	I (MA)	B (T)	P_{NB} (MW)	δ	n_{eped} (e19/m^3)	T_{eped} (eV)	$P_{sep}^{exp,b}$ (MW)	P_{thr}^{c} (MW)
102456	1725	1.4	2.0	2.6	0.73	3.22	95	1.55-1.86	1.54
97979	1900	1.4	2.0	2.0	0.79	2.59	125	1.72-2.04	2.18
92079	2275	1.0	2.1	6.8	0.37	1.28	220	3.99-4.06	4.00
84027	2575	1.3	2.1	1.1	0.32	2.94	144	1.28-1.36	1.13
97979[a]	3250	1.4	2.0	6.5	0.79	6.35	525	4.64-4.96	2.59

[a] well into H-mode phase, not at the L-H transition—control case

[b] experimental non-radiative power across separatrix (range reflects uncertainty in $P_{radcore}$)

[c] prediction of power threshold for stabilization of thermal instabilities

We recall the previous finding[4] that the same power threshold expression predicts values in good agreement with measured non-radiative power crossing the separatrix just prior to a H-L back transition for a set of 'density limit' shots with core radiative power fractions of 20-40%. These findings combine to provide a strong suggestion that stabilization of thermal instabilities in the edge pedestal plays a major role in triggering the L-H transition and that destabilization plays a similar role in triggering the back H-L transition.

Even broader experimental support for the stabilization of thermal instabilities as a trigger mechanism for the L-H transition may be inherent in the recent finding[4] that edge gradients in temperature and pressure may be better control parameters for predicting the L-H transition than the edge values of the temperature or pressure. The temperature and pressure gradients, but not the electron density gradient, all measured in the region in which the H-mode pedestal ultimately formed, were found to increase during the L-mode phase in shots which made a H-mode transition. This is consistent

with the predicted thermal instability stabilization due to increasing temperature gradients as the threshold power is approached that was discussed in Ref. 1.

To put these results in perspective, we note that the L-H transition has been studied experimentally for more than a decade (e.g. Refs. 5-9) and that the reigning paradigm for the L-H transition that has emerged is the suppression of turbulent transport by the sheared ExB flow produced by a sharp gradient in the negative radial electric field just inside the separatrix. Triggering mechanisms previously put forward to account for the creation of this local radial electric field shear include orbit loss[10] and Stringer spin-up[11]. It has been suggested[1] that the reduced transport that occurs when the power threshold of Eq. (1) is exceeded produces a reduced particle flux across the separatrix (supported by D_α measurements) that in turn produces a positive poloidal rotation (as observed) that results via momentum balance in a negative radial electric field. Thus, the thermal instability suppression mechanism[1], the threshold power prediction of which was confirmed in this paper and in Ref. 3, provides another possible explanation for the trigger mechanism for L-H and H-L transitions.

A paper has been prepared for Physics of Plasmas.

1. W. M. Stacey, Phys. Plasmas, 9, 3082 (2002).
2. W. M. Stacey, Phys. Plasmas, 6, 2452 (1999).
3. W. M. Stacey and T. W. Petrie, Phys. Plasmas, 10, 3349 (2003).
4. R. J. Groebner, D. M. Thomas and R. D. Deranian, Phys. Plasmas, 8, 2722 (2001).
5. E. J. Doyle, R. J. Groebner, K. H. Burrell*, et al.*, Phys. Fluids B, 3, 2300 (1991).
6. R. J. Groebner, Phys. Fluids B, 5, 2343 (1993).
7. K. H. Burrell, E. J. Doyle, P. Gohil, *et al*., Phys. Plasmas, 1, 1536 (1994).
8. K. H. Burrell, Phys. Plasmas, 4, 1499 (1997).
9. R. J. Groebner, D. R. Baker, K. H. Burrell, *et al.*, Nucl. Fusion, 41, 1789 (2001).
10. K. C. Shaing and E. C. Crume, Phys. Rev. Lett., 63, 2369 (1989); K. C. Shaing, E. C. Crume and W. A. Houlberg, Phys. Fluid B, 2, 1492 (1990).
11. A. B. Hassam, T. M. Antonsen, J. F. Drake and C. S. Liu, Phys. Rev. Lett., 66, 309 (1991).

C. NEUTRAL TRANSPORT

(J. Mandrekas, W. M. Stacey, R. J. Colchin, T. W. Petrie)

The Transmission/Escape Probability (TEP) 2-D neutral transport code GTNEUT is a computationally efficient alternative to traditional Monte Carlo methods. Recent implementation of a realistic wall reflection model allowed us to analyze DIII-D neutral density measurements and to benchmark GTNEUT against both Monte Carlo and experiment[1].

GTNEUT was recently upgraded with new capabilities which greatly facilitated setting up and performing DIII-D neutral transport simulations. These upgrades included: a) the implementation of a high performance sparse matrix solver for the solution of the

linear system of neutral transport equations, which allows us to run much larger and geometrically detailed problems and b) the development of an interface routine that can prepare the geometric part of the GTNEUT input file (which is the most laborious part) automatically by directly reading EFIT EQDSK files.

To illustrate the capabilities of the upgraded code, we used it to calculate the exhaust rates from the dome and baffle pumps for the DIII-D shot 113026 @ 3000 ms (an upper single null discharge with dRsep ≈ 1.2, part of the AT Divertor Pumping series of experiments). The upper part of the model geometry is shown in Fig.1 (we actually modeled the entire plasma chamber to exercise the code). For the background plasma parameters (electron and ion densities and temperatures) inside the separatrix, we assumed poloidal symmetry and used the values obtained from GAProfiles. For the plasma parameters in the SOL above and below the X-point, we used other experimental data. For the regions where experimental data were unavailable (private flux region and the near-vacuum regions between the first wall and the last open flux surface) we assigned plausible background plasma parameters.

The results of the neutral transport simulations depend on the ion and neutral recycling assumptions. Since no detailed information on the location and magnitude of the recycling sources was available for this shot, our reference simulation assumed in/out symmetry and equal recycling sources from the four wall segments (84, 86, 93, 95) adjacent to the dome and baffle pump entrances (segments 85 and 94) in Fig. 1. This is a reasonable assumption given the flux expansion between the X-point and the strike points and the experimental indication of comparable recycling rates from inside and outside. The magnitude of the recycling sources was based on a crude estimate from the in/out ion flows at the pre-sheath, but the magnitude is not important since the transport problem is linear and we were interested in the ratio of the exhaust rates (the neutral fluxes to segments 85 and 94). For this reference case, $\Gamma_{dome} / \Gamma_{baffle} = 0.88$ was calculated, in quite good agreement with the ratio of measured exhaust rates.

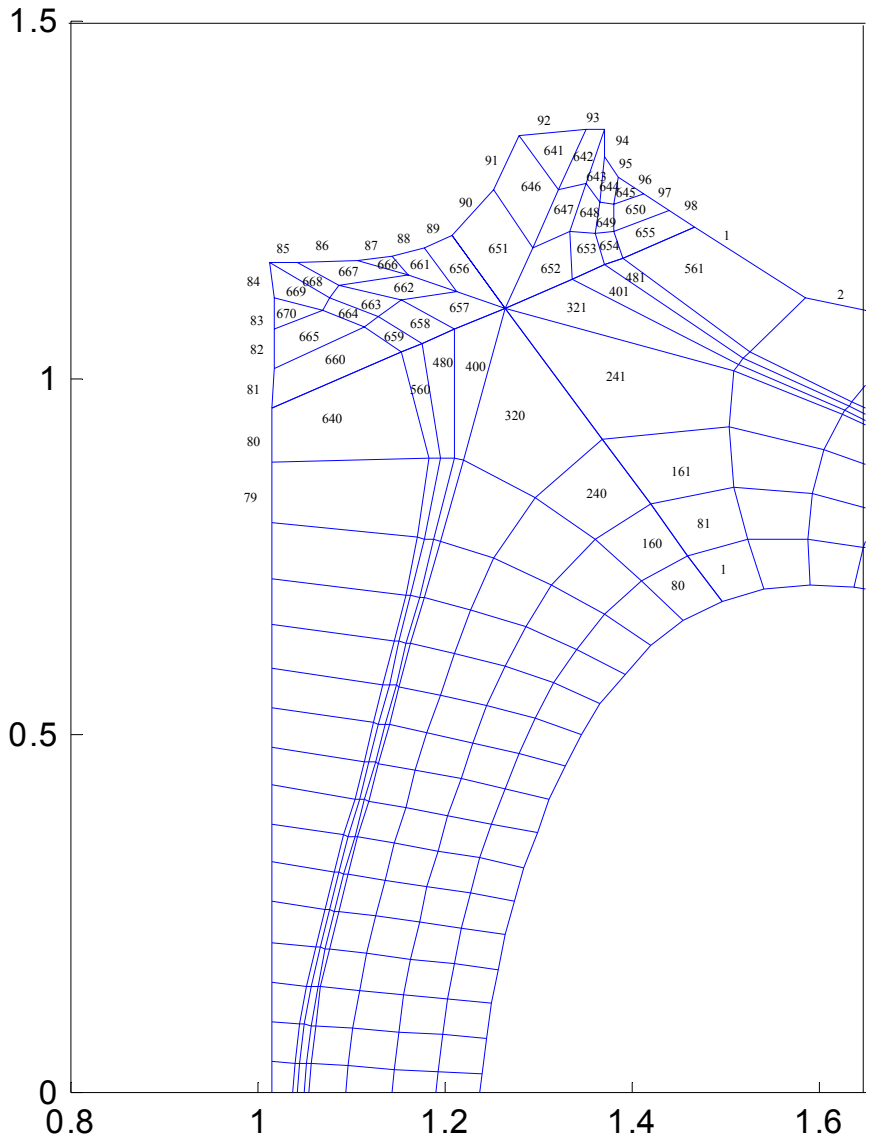

The

Figure 4: Upper part of DIII-D geometry used by GTNEUT for the analysis of DIII-D shot 113026 @ 3000 ms. The dome and baffle pump openings are represented by wall segments 85 and 94 respectively.

To illustrate how the GTNEUT code can be used to test recycling hypotheses, the $\Gamma_{dome} / \Gamma_{baffle}$ ratio was calculated for uniform recycling from the main chamber wall (the second case in Table 1) and for various combinations of recycling flux ratios among the various regions near the divertor strike points. These results are shown in Table 1. It can be seen that the $\Gamma_{dome} / \Gamma_{baffle}$ ratio is a sensitive function of the location of the recycling source and perhaps could be used as a diagnostic of the recycling location.

Table 1: Sensitivity of the $\Gamma_{dome} / \Gamma_{baffle}$ ratio to various recycling assumptions. The total recycling source is kept constant for all cases and equal to 1.0×10^{23} #/s. Numerical subscripts correspond to the GTNEUT wall numbering scheme (see Fig. 1).

Flux distribution	Γ_{dome} **(#/s)**	Γ_{baffle} **(#/s)**	$\Gamma_{dome} / \Gamma_{baffle}$
$\Phi_{84} = \Phi_{86} = \Phi_{93} = \Phi_{95}$	0.5695×10^{22}	0.6426×10^{22}	**0.88**
Uniform (MCR)	0.613×10^{21}	0.71×10^{21}	**0.86**
$\Phi_{86} = \Phi_{93}$, $\Phi_{84} = \Phi_{95} = 0$	0.192×10^{22}	0.924×10^{22}	**0.20**
$\Phi_{86} = 1.5\times\Phi_{84}$ $\Phi_{93} = \Phi_{95}$	0.494×10^{22}	0.643×10^{22}	**0.76**
$\Phi_{in} / \Phi_{out} = 0.5$	0.380×10^{22}	0.855×10^{22}	**0.45**
$\Phi_{in} / \Phi_{out} = 2.0$	0.760×10^{22}	0.430×10^{22}	**1.77**

1. J. Mandrekas, R. J. Colchin, W. M. Stacey, et al., Nucl. Fusion, **43**, 314 (2003).

D. ROTATION

(J. Mandrekas and W. M. Stacey)

We have previously compiled[1] and successfully tested against DIII-D data[2] a neoclassical model for the calculation of plasma rotation and gyroviscous momentum transport. The calculation model consists of a coupled set of non-linear momentum balance equations for the toroidal and poloidal velocities and the sine and cosine components of the density asymmetry over the flux surface for each ion species present (2 in our present model). We have reviewed the derivation of these various equations to make field and current direction explicit in the formalism and to avoid making certain series expansions that could lead to inaccuracies under certain extreme conditions. We are now in the process of developing and testing robust solution procedures for this nonlinear set of equations.

This work was reported at APS-DPP-03.

1. W. M. Stacey, Phys. Plasmas, 8, 158 (2001).
2. W. M. Stacey and J. Mandrekas, Phys. Plasmas, 9, 1622 (2002).

III. THEORY, ANALYSIS AND CODE DEVELOPMENT

A. NEUTRAL PARTICLE TRANSPORT

Extensions of the TEP methodology

(Dingkang Zhang, J. Mandrekas, W.M. Stacey)

Extensive comparisons of GTNEUT predictions against Monte Carlo calculations and experimental measurements in DIII-D, have demonstrated the accuracy and computational efficiency of the TEP method for a wide range of conditions. However, calculations of detailed model problems designed to test approximations in limiting cases have identified two main areas in which extensions in the original TEP methodology would be useful: 1) taking anisotropy into account in the calculation of first-flight transmission coefficients when the neutral mean free path (mfp) is much larger than the characteristic dimension of the computational region; and 2) taking into account that the escape of scattered or charge-exchanged neutrals is preferentially across the incident surface when the mfp is small compared to the characteristic dimension of the computational region.

The TEP methodology has been recently extended[1] to address the above issues. To improve the accuracy of the TEP method in cases where the neutral distribution function at the interfaces is expected to be anisotropic, the original DP_0 approximation was extended to include linearly (DP_1) and quadratically (DP_2) anisotropic distributions.

Benchmarking calculations with Monte Carlo indicate that the DP_1 calculation is significantly better than the original DP_0 calculation for model problems chosen to accentuate anisotropy, but there is little advantage to further extending the calculation to DP_2. This is shown in Fig. 5, where the neutral densities predicted by the DP_0, DP_1, and DP_2 approximations in GTNEUT are compared with the DEGAS Monte Carlo code for a one-dimensional model problem in a purely ionizing medium (charge exchange fraction $c = 0$) and with a mfp to grid size ratio λ/Δ equal to 0.5.

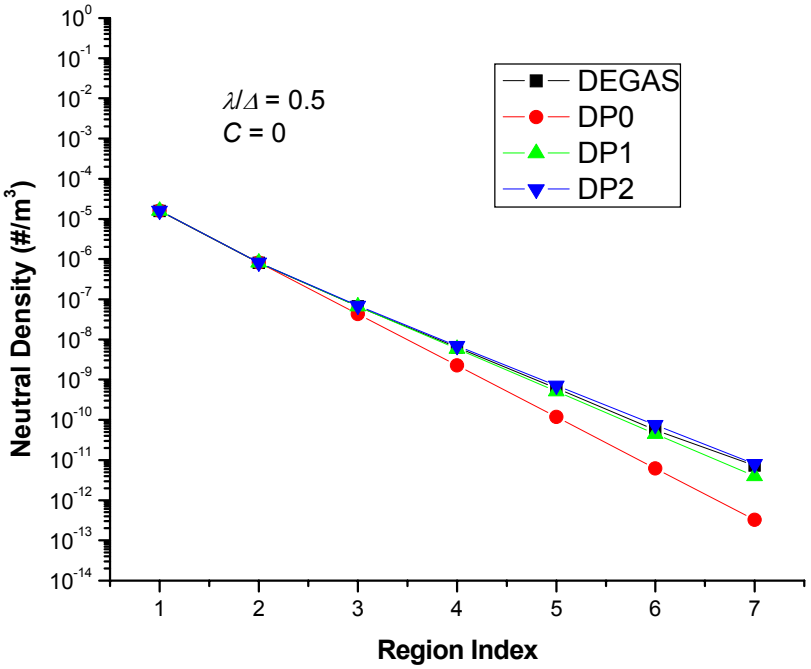

Figure 5: Comparison of neutral density attenuation in a 1-D plane configuration for different approximations.

Work is also underway to address the second of the issues identified above, i.e. the potential inaccuracy of the TEP methodology in regions of small neutral mfp relative to the characteristic dimensions of the region, due to strong non-uniformities in the first collision charge exchange source.. Our first approach has been to introduce a correction to the directional escape probability term based on the *albedo* coefficient[1]. This was suggested by the fact that if the neutral mfp is much smaller than the characteristic dimension of a region, we can treat it as an infinite half space and express the fraction of the collided particles that is scattered back across the incident surface in terms of the albedo coefficient**.** Preliminary simulations and benchmarks with Monte Carlo are encouraging[1].

LLNL Collaboration

(J. Mandrekas, Dingkang Zhang, M. Umansky, T. Rognlien)

The computational speed of the GTNEUT code as well as the deterministic nature of the TEP methodology which leads to noise-free simulations, make GTNEUT an ideal code for coupling with 2-D fluid edge codes. Since the 2D edge fluid code UEDGE is the predominant edge fluid code used in US fusion laboratories, the coupling of the GTNEUT and UEDGE codes has always been an eventual goal of our code development effort.

Following preliminary discussions with the developers of the UEDGE code at LLNL, we have undertaken a series of testing and benchmarking simulations between the GTNEUT code and the fluid neutral model of UEDGE. The goal of these simulations, which are being carried out with the collaboration of Maxim Umansky of LLNL, is to ascertain the strengths of the GTNEUT code vis-à-vis UEDGE's existing fluid neutrals model for a variety of background plasma conditions and, especially, for those conditions where the fluid approximation for the neutrals is expected to be invalid. The results of these simulations will help us decide whether to proceed to the next step, i.e. the implementation of GTNEUT as a routine in the UEDGE code.

1. Dingkang Zhang, J. Mandrekas, and W. M. Stacey, "Extensions of the TEP neutral transport methodology," to be published in *Contrib. Plasma Phys*., 2004.

B. TOROIDAL ROTATION AND RADIAL ELECTRIC FIELD IN EDGE PEDESTAL (W. M. Stacey)

A model for ion toroidal velocities and the radial electric field in the edge pedestal region of tokamaks has been developed. The model is based on particle and momentum balance and incorporates the neoclassical gyroviscous toroidal viscous force. The toroidal rotation is driven by the input beam torque ($RM_{\varphi j}$), the input torque associated with the induced field ($Rn_j e_j E_\varphi$), and by the internal torque due to the radial ion flow ($e_j B_\theta \Gamma_j$), and depends on the radial transfer rate of toroidal angular momentum (ν_{dj}*) due to viscous, atomic physics and convective effects and on the interspecies momentum exchange rate (ν_{jk}). The local electric field depends on the total local input momentum deposition ($M_\varphi = \Sigma_j M_{\varphi j}$), the local radial pressure gradients (P_j'), the local poloidal velocities ($\upsilon_{\theta j}$) and the local values of the radial momentum transfer rates (ν_{dj}*) due to viscous, atomic physics and convective effects.

This calculation model predicts carbon toroidal rotation velocities in the DIII-D edge pedestal to within about a factor of 2 or better, for a wide range of edge pedestal parameters. This result is consistent with the recent observation[1] that the measured momentum transport frequency through the edge pedestal was within about a factor of 2 of the neoclassical gyroviscous prediction, over this same set of edge pedestal conditions. These results provide a measure of confidence in the calculation model for toroidal rotation in the edge pedestal that was presented in this paper.

A paper has been prepared and submitted to Physics of Plasmas[1].

1. 1. W. M. Stacey, "Investigation of Transport in the DIII-D Edge Pedestal", Phys. Plasmas, submitted (2003).